supported by Natural Sciences and Engineering Research Council of CanadaDiscovery grant 402792 and Canadian School of Energy and Environment Proof of Principle Grant. The ellipsometric measurements were carried out at the Center for Functional Nanomaterials at Brookhaven National Laboratory, which is supported by the U.S. Department of Energy, Office of Basic Energy Sciences, under contract DE-AC02-98CH10886.

Supplementary Materials
www.sciencemag.org/cgi/content/full/336/6078/205/DC1
Materials and Methods
Figs. S1 to S6
References (*29*, *30*)

16 January 2012; accepted 7 March 2012
10.1126/science.1219171

Ferroelectric Columnar Liquid Crystal Featuring Confined Polar Groups Within Core–Shell Architecture

Daigo Miyajima,[1] Fumito Araoka,[2] Hideo Takezoe,[2]* Jungeun Kim,[3] Kenichi Kato,[4] Masaki Takata,[3,4] Takuzo Aida[1]*

Ferroelectric liquid crystals are materials that have a remnant and electrically invertible polar order. Columnar liquid crystals with a ferroelectric nature have potential use in ultrahigh-density memory devices, if electrical polarization occurs along the columnar axis. However, columnar liquid crystals having an axial nonzero polarization at zero electric field and its electrical invertibility have not been demonstrated. Here, we report a ferroelectric response for a columnar liquid crystal adopting a core–shell architecture that accommodates an array of polar cyano groups confined by a hydrogen-bonded amide network with an optimal strength. Under an applied electric field, both columns and core cyano groups align unidirectionally, thereby developing an extremely large macroscopic remnant polarization.

Ferroelectric liquid crystals (FLCs) have potential application in lightweight, easy-processable electrical devices for fast-switching displays, rewritable memories, and nonlinear optics (*1*). For liquid crystalline (LC) materials to operate ferroelectrically, a nonzero polarization at zero electric field (E-field), together with its electrical invertibility, is a prerequisite. However, this goal is difficult to realize, particularly in dynamic molecular systems such as LC materials, as once oriented electrically, polar motifs reorganize spontaneously at zero E-field in such a way that their dipoles cancel each other either macroscopically or locally. Although FLCs with a smectic geometry (Fig. 1, A and B) have been reported (*2*–*5*), most require cell

[1]Department of Chemistry and Biotechnology, School of Engineering, The University of Tokyo, 7-3-1 Hongo, Bunkyo-ku, Tokyo 113-8656, Japan. [2]Department of Organic and Polymeric Materials, Tokyo Institute of Technology, 2-12-1 O-okayama, Meguro-ku, Tokyo 152-8552, Japan. [3]Japan Synchrotron Radiation Research Institute (JASRI), 1-1-1 Kouto, Sayo-cho, Sayo-gun, Hyogo 679-5148, Japan. [4]RIKEN SPring-8 Center, 1-1-1 Kouto, Sayo-cho, Sayo-gun, Hyogo 679-5148, Japan.

*To whom correspondence should be addressed. E-mail: takezoe.h.aa@m.titech.ac.jp (H.T.); aida@macro.t.u-tokyo.ac.jp (T.A.)

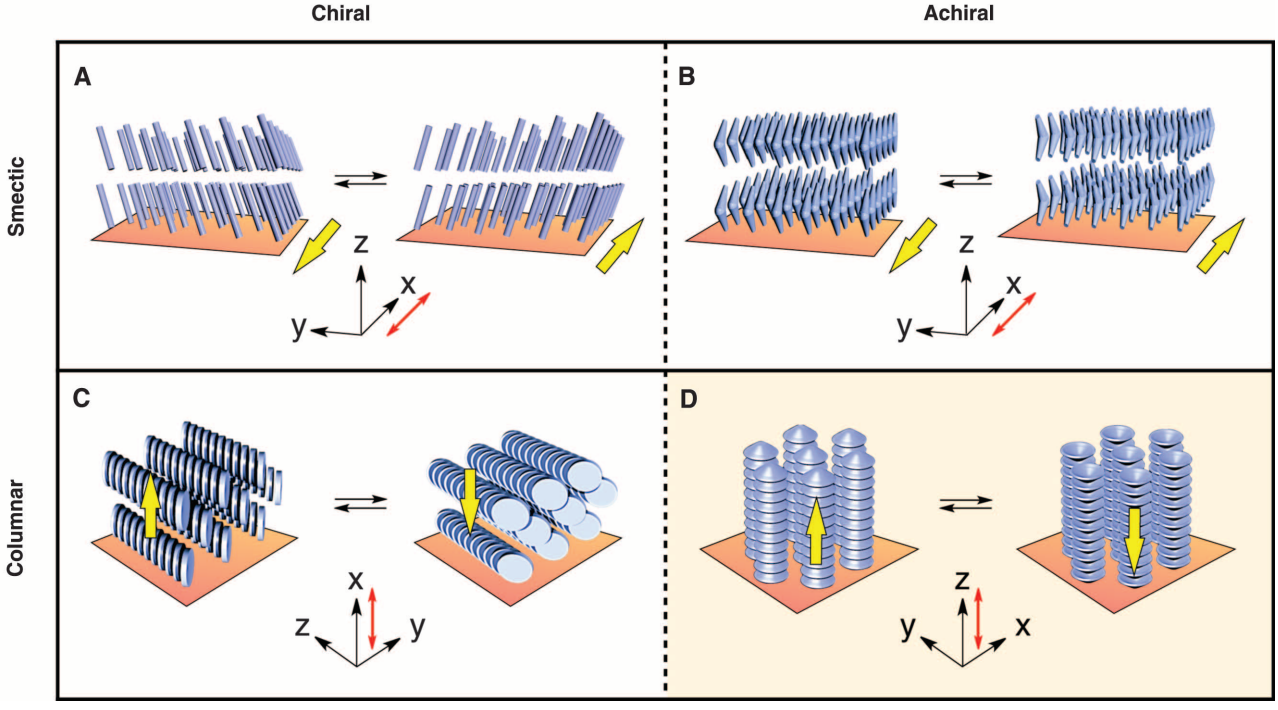

Fig. 1. Schematic illustrations of the electrical polarization behaviors of ferroelectric liquid crystals (FLCs) with four different geometries. (**A**) and (**B**) illustrate the behaviors of smectic-type FLCs consisting of chiral rod-shaped and achiral bent-shaped molecules, respectively, whereas (**C**) and (**D**) represent those of columnar FLCs composed of chiral discotic and achiral umbrella-shaped molecules, respectively. Red and yellow arrows denote the directions of an applied electric field (E-field) and the resulting polarization, respectively. Chiral rod-shaped molecules generate a layer polarization in the *x*-*y* plane. However, no macroscopic polarization develops because such a layer polarization is canceled owing to its helical orientation with the helical axis along the *z* direction. To develop a macroscopic polarization, a thin cell has been used so that an enhanced cell-surface effect unwinds the helical geometry as shown in (A). Achiral bent-shaped molecules, which likewise generate a layer polarization in the *x*-*y* plane, do not assemble in a helical geometry, so that a macroscopic polarization develops as shown in (B). Columnarly assembled chiral discotic molecules adopt a helical geometry, which generates a polarization in a perpendicular direction (*x* direction) to the columnar axis when the helical geometry is unwound by means of a cell-surface effect as shown in (C). In contrast to (A) to (C), columnarly assembled achiral umbrella-shaped molecules (this work) generate a polarization along the columnar axis (*z* direction). Therefore, unidirectional orientation of such columns results in the development of a macroscopic polarization as shown in (D).

surfaces to help maintain an electrically generated macroscopic polarization at zero E-field (*6*–*8*). To date, columnar FLCs, having a remnant and electrically invertible axial polarization (Fig. 1D), have not been demonstrated. Although some columnar LCs develop an electrically invertible axial polarization (*9*, *10*), they lose the polarization within a millisecond (*10*, *11*) when the applied E-field is turned off. Even when the structural relaxation is observed to be slow, the polarization disappears only within ~100 s (*12*) after the E-field has been turned off. Further-

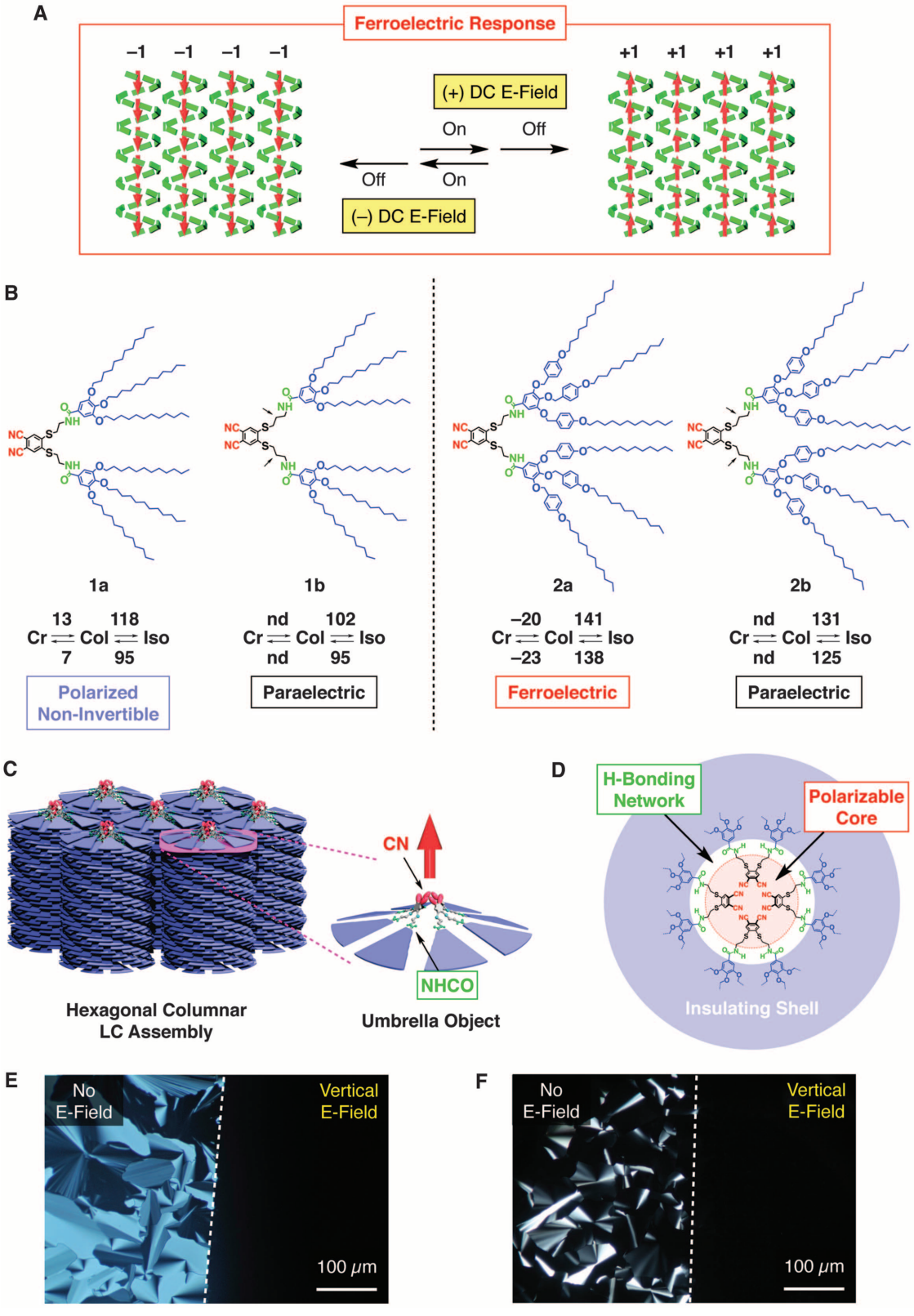

Fig. 2. Schematic illustration of (**A**) the ferroelectric response of electrically polarizable columns of **2a**. Red arrows and green squares represent an array of cyano groups and a hydrogen-bonded amide network, respectively. (**B**) Schematic illustrations of the molecular structures of compounds **1a** (*14*), **1b** (*14*), **2a**, and **2b** (arrows highlight the extra methylene group in **1b** and **2b**). Numerical values in phase diagrams represent phase-transition temperatures (°C), where Cr, Col, and Iso denote crystalline, hexagonal columnar, and isotropic phases, respectively (nd, not determined by DSC measurements). (**C** and **D**) Schematic illustrations of (C) columnarly assembled fan-shaped molecules and (D) a cross-section of their core–shell columnar assembly. (**E** and **F**) POM images of LC films of (E) **2a** at 120°C and (F) **2b** at 110°C under crossed polarizers. Samples were filled in a sandwich-type glass cell (thickness, 5 μm) equipped with patterned indium tin oxide (ITO) electrodes, which allowed an AC E-field (1.0 Hz, 20 V_{pp} μm^{-1}) to operate site-selectively from a vertical direction relative to the film sample. Dashed lines mark the border between E-field operating and nonoperating areas. In dark-view areas sandwiched by ITO electrodes, LC columns are oriented vertically.

more, unlike smectic FLCs, no columnar LCs are known to stabilize an electrically induced polarization along their columnar axes with the aid of cell surfaces. Here, we address a long-standing question of how to develop a ferroelectric response in a columnar architecture. Columnar FLCs having an axial nonzero polarization at zero E-field and its electrical invertibility (Fig. 1D) are considered candidate materials for ultrahigh-density memory devices, as individual columns, when vertically aligned with respect to the electrodes, could ultimately serve as a one-bit memory (*13*, *14*). If electrical polarization occurs in a direction perpendicular to the columnar axis (Fig. 1C) (*15*), such an ultrahigh-density memory device cannot be achieved. Thus, the goal of achieving columnar FLCs with an axial polarization (Fig. 1D) remains unresolved (*16*–*20*).

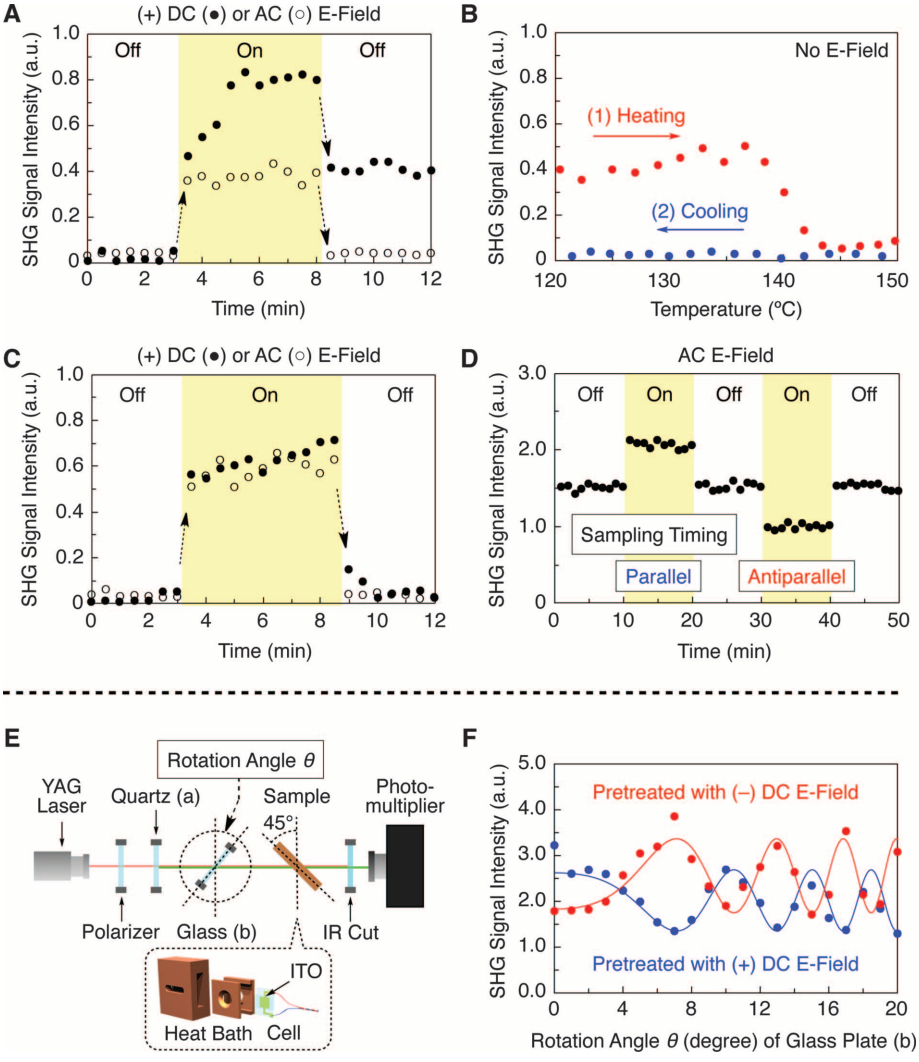

Fig. 3. (**A** and **C**) Effects of DC (10 V μm^{-1}; filled circles) and AC (10 Hz, 20 V_{pp} μm^{-1}; open circles) E-fields on oriented LC films (thickness, 5 μm) of (A) **2a** at 120°C and (C) **2b** at 110°C, as observed by second-harmonic generation (SHG). (**B**) Thermal SHG profiles of a sample, obtained in (A) by use of a DC E-field (10 V μm^{-1}), upon (1) heating up to an isotropic phase (red circles), followed by (2) cooling to the LC mesophase (blue circles) in the absence of an E-field. Once the LC sample lost its SHG activity on phase transition to the isotropic phase, macroscopic polar order did not emerge until the resulting material was allowed to transform back to the LC mesophase by cooling and polarized by applying a DC E-field. (**D**) Effect of an AC E-field (10 Hz, 20 V_{pp} μm^{-1}), as observed by SHG at 120°C, on an oriented LC film (thickness, 5 μm) of **2a**, polarized beforehand by applying a DC E-field (10 V μm^{-1}) at 120°C. "Parallel" and "antiparallel" indicate that the data sampling was synchronously made when the switching AC E-field was directed parallel and antiparallel, respectively, to the DC E-field used for polarizing the sample. (**E** and **F**) SHG interferometry of an oriented LC film (thickness, 5 μm) of **2a**, polarized before the measurements by applying a DC E-field (10 V μm^{-1}) at 120°C. (E) Schematic illustration of the optical setup for SHG interferometry. (F) SHG interferograms at different rotation angles (θ) of a glass plate (b) in (E) at 120°C. Samples that gave blue and red data points were polarized beforehand at 120°C with (+) and (–) DC E-fields, respectively. Solid curves were obtained by theoretical fitting. IR, infrared; YAG, yttrium-aluminum-garnet.

Here we report a columnar LC that can electrically develop a polarization along the columnar axis and maintain its polar order over a wide temperature range below the clearing temperature (Fig. 2A). Furthermore, this remnant polarization can be electrically inverted at a rather low coercive field (2.3 kV cm^{-1}), where the magnitude of spontaneous polarization is much larger (P_s ~5.0 μC cm^{-2}) than those of current smectic FLCs (P_s < 1.0 μC cm^{-2}). Our molecular design uses fan-shaped **2a** (Fig. 2B) carrying a polar phthalonitrile head group that anchors tapered paraffinic wedges via a hydrogen-bonding amide linker. This molecule self-assembles into an umbrella-shaped object (*21*, *22*) with polar cyano groups inside, which stacks up columnarly via hydrogen-bonding and van der Waals interactions at the amide and paraffinic parts, respectively (Fig. 2, C and D). The hydrogen-bonded amide network is developed along the columnar axis and ensures a core–shell architecture, where a large paraffinic shell wraps around a polarizable core domain accommodating an array of cyano groups. This core–shell architecture (Fig. 2D) was inspired by our recent work on E-field–responsive columnar LCs (*23*). We developed a particular type of "amide handle" that imparts an E-field–orientable nature to a variety of columnar LCs. In these cases, electrical orientation of the amide handles, by means of an alternating-current (AC) E-field, gives rise to large-area unidirectional orientation of LC columns along the field direction; however, none were ferroelectrically polarizable. Nevertheless, the LC mesophase of compound **1a** (Fig. 2B), which carries smaller paraffinic wedges than **2a**, has an intrinsic polarization, although its direction cannot be electrically inverted. We hypothesized that the inability to invert polarization may be due to a highly congested environment of the core part. Thus, compound **1b** (Fig. 2B), bearing amide linkers with one more carbon than **1a**, was synthesized in order to expand the core part appropriately. However, with such a small structural modification, the resulting columnar LC behaved paraelectrically.

In this study, we increased the shell volume of the core–shell architecture so that the hydrogen-bonded amide network, which confines the polarizable core, might become looser. We synthesized fan-shaped **2a** together with **2b** as a core-expanded reference (Fig. 2B) (*24*). By means of differential scanning calorimetry (DSC) (fig. S5), polarizing optical microscopy (POM; Fig. 2, E and F), and x-ray diffraction (XRD; fig. S7) analysis, we confirmed that both compounds self-assemble into a hexagonal columnar LC mesophase over a wide temperature range, including room temperature (phase diagrams in Fig. 2B). The intercolumnar distances,

as determined from the observed XRD patterns, indicate that their columnarly stacked elemental motifs are umbrella-shaped (*25*). Furthermore, when a 1.0-Hz square-shaped AC E-field [20 V peak-to-peak (V_{pp}) μm^{-1}] was applied site-selectively in a vertical direction, the LC films (thickness, 5 μm) under crossed polarizers displayed a dark view in an E-field–operating area (Fig. 2, E and F). Thus, these columnar LCs can be electrically oriented.

FLCs should show a nonzero polarization at zero E-field, as well as electrical polarization switching. However, even nonferroelectric LCs, if contaminated with ionic species or if they relax slowly from an electrically polarized state, may display a switching profile that could be confused with ferroelectricity. Therefore, as in the case of **1a**, we investigated LC samples of **2a** and **2b** using second-harmonic generation (SHG), which provides a convenient and reliable method for optically demonstrating the existence of a polar order at zero E-field (*26*, *27*). However, regardless of whether their columns were preoriented by an AC E-field, neither **2a** nor **2b** showed an intrinsic SHG activity (Figs. 3, A and C, 0 to 3 min). Hence, we decided to explore the effects of a direct-current (DC) E-field (10 V μm^{-1}) on the polarization of these LC materials. Surprisingly a macroscopic polarization was electrically induced in a film sample (thickness, 5 μm) of **2a** and was maintained after the applied E-field was turned off. The SHG signal appeared as soon as the DC E-field was applied to the sample (Fig. 3A, filled circles) then gradually intensified, reaching a plateau in 3 min. When the DC E-field was turned off, a certain amount of the SHG activity was lost. However, the material still remained SHG-active. By contrast, when an AC E-field (10 Hz, 20 V_{pp} μm^{-1}) was applied (Fig. 3A, open circles), SHG activity developed abruptly but was completely lost after the E-field was turned off. These observations allow us to conclude that the LC assembly of **2a** is macroscopically polarizable by a DC E-field. Notably, the induced polarization is thermally stable and maintained up to the clearing temperature for the LC mesophase (Fig. 3B, red circles).

We used SHG interferometry (*28*) to examine if the induced polarization in **2a** is electrically invertible. The optical setup (Fig. 3E) was configured so that SHG, if any, from a sample in question could interfere with that from a quartz plate (a). Thus, when a glass plate (b) is rotated, a phase shift is induced between the incident SHG beam from a quartz plate and the incident fundamental beam. Consequently, these SHG beams interfere constructively or destructively depending on the rotation angle, resulting in the development of a fringe pattern. Indeed, when the LC film of **2a** (thickness, 5 μm) was polarized before the measurement by applying a DC E-field (+10 V μm^{-1}) at 120°C, an interference fringe emerged (Fig. 3F). Notably, when the LC film was likewise pretreated in the opposite direction with the DC E-field (–10 V μm^{-1}), a mirror-image fringe pattern (Fig. 3F; blue and red lines) developed. Therefore, we conclude that **2a** gives rise to a ferroelectric response in its columnar assembly (Fig. 2A). By contrast, the SHG profiles of core-expanded **2b** under AC (Fig. 3C, open circles) and DC (Fig. 3C, filled circles)

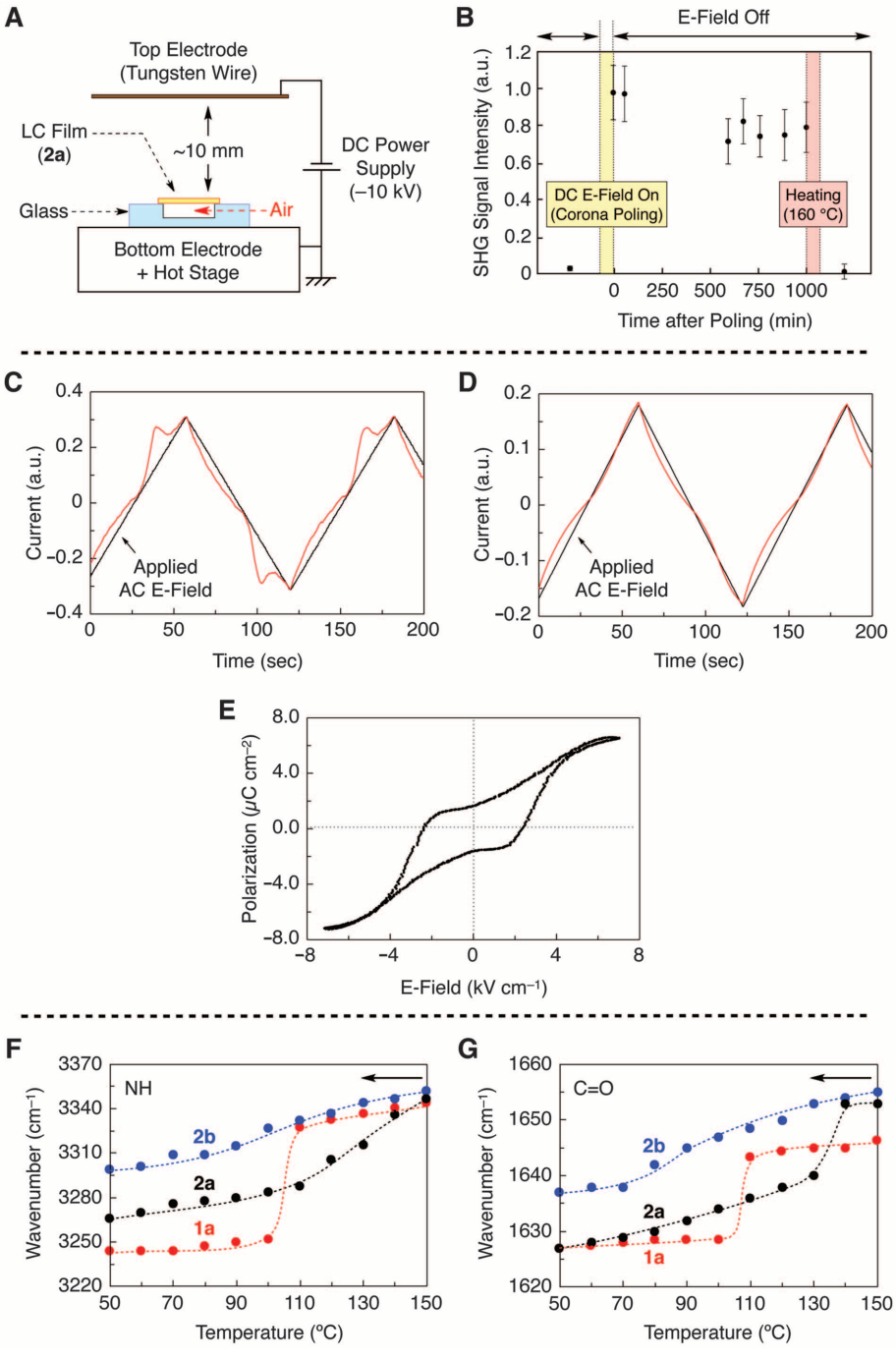

Fig. 4. (**A** and **B**) Effects of a DC E-field (corona poling; 1.0 kV mm^{-1}) on a free-standing LC film (thickness, ~8 μm) of **2a** at 120°C, as observed by SHG. (**A**) Schematic illustration of the optical setup for corona poling. (B) SHG profiles of the sample measured at 60°C before and after corona poling at 120°C for 30 min, followed by heating to 160°C for 15 min and then cooling to 60°C in the absence of an E-field. (**C** and **D**) Polarization reversal current profiles (red curves) of oriented LC films (thickness, 5 μm) of (C) **2a** at 120°C and (D) **2b** at 110°C on application of a triangular-shaped AC E-field (0.008 Hz, 20 V_{pp} μm^{-1}, black lines). (**E**) *P-E* hysteresis loop of an oriented LC film (thickness, 5 μm) of **2a** at 120°C, obtained by integration of the current profile in (C). (**F** and **G**) Infrared spectral change profiles at (F) 3370 to 3220 cm^{-1} (NH) and (G) 1660 to 1620 cm^{-1} (C=O) of **1a** (red circles), **2a** (black circles), and **2b** (blue circles) through the isotropic-to-LC phase transition.

E-fields indicated that the LC material in either case is polarized only temporarily, as in the case of **2a** under the influence of an AC E-field (Fig. 3A, open circles). Thus, the columnar LC assembly of **2b** is not ferroelectric but rather paraelectric. Unlike that of most smectic LCs, the ferroelectric nature observed for the columnar LC assembly of **2a** is "genuine" in that the electrically induced macroscopic polarization is maintained solely by its chemical architecture without the need for substrate-induced physical perturbations from cell surfaces. Indeed, when a DC E-field was applied to a free-standing LC film of columnarly assembled **2a** (corona poling, Fig. 4A), SHG activity emerged and was maintained unless the sample was heated above the clearing temperature for the LC mesophase (Fig. 4B).

For device applications, coercive electric field (E_c) and magnitude of polarization (P_s), together with remnant polarization (P_r), are important parameters (*29*, *30*). For evaluating these parameters, a triangular-shaped AC E-field (20 V_{pp} μm^{-1}) was applied at 120°C to an oriented LC film (thickness, 5 μm) of **2a**. When the AC E-field frequency was in the range of 10 to 0.1 Hz, only featureless current profiles resulted (fig. S8), indicating that the electrical inversion of polarization is hardly induced. However, when the AC E-field frequency was further reduced (e.g., to 0.008 Hz), the sample started to display current peaks (Fig. 4C) as a result of the inversion of polarization. Integration of the observed current profile afforded a *P*-*E* loop with a clear hysteresis feature (Fig. 4E) typical of ferroelectric materials, where E_c, P_s, and P_r were evaluated as 2.3 kV cm^{-1}, 5.8 μC cm^{-2}, and 1.7 μC cm^{-2}, respectively. Notably, the E_c thus observed is much smaller than those of ferroelectric polymers. Furthermore, the observed P_s is larger than the highest P_s values (<1.0 μC cm^{-2}) so far reported for ferroelectric LC materials with a smectic geometry, although the value may contain a small margin of error due to a baseline fluctuation in Fig. 4C. By contrast, core-expanded **2b**, as expected from its paraelectric SHG response (Fig. 3C), displayed a nearly featureless current profile over a wide range of the applied E-field frequency (Fig. 4D).

Comparison of the structures of four fan-shaped LC molecules in Fig. 2B shows that the ferroelectric nature of **2a** results from a delicate balance between the structural factors involved in the core and shell domains of the columnar assembly. Namely, the polar cyano groups, which are confined in the core domain of the column, are congested in such a way that their E-field–induced orientation, leading to a polarization along the columnar axis, can be maintained after the E-field is turned off. The core environment in prototype **1a** seems to be too congested for the cyano groups to respond electrically, whereas those of core-expanded **1b** and **2b** are too flexible to maintain the induced orientation of the cyano groups. We consider that the ferroelectric columnar assembly of **2a** could possess a slightly looser hydrogen-bonded amide network than prototype **1a** because of the accommodation of larger paraffinic wedges in the shell domain. To support this hypothesis, we investigated the infrared spectral change profile of **2a** associated with the isotropic-to-LC phase transition, together with those of prototype **1a** and core-expanded **2b** as references. As expected from the three-dimensional structural order in its LC mesophase, prototype **1a** upon phase transition displayed an abrupt spectral change at the NH (Fig. 4F, red) and C=O (Fig. 4G, red) stretching vibrational bands. By contrast, the corresponding spectral change in core-expanded **2b** was quite gradual; the stretching vibrational bands due to C=O and NH shifted almost monotonically toward a lower wavenumber region (Fig. 4, F and G, blue dashed curves). Furthermore, the wavenumbers of these vibrational bands were obviously larger than those of **1a** in the LC mesophase. Therefore, the hydrogen-bonded amide network is much less developed and more labile than that in **1a**. Meanwhile, in agreement with our hypothesis, **2a** displayed a moderate spectral change profile between those of the two reference compounds (Fig. 4, F and G, black dashed curves), where the wavenumbers of its C=O and NH vibrational bands are present in-between those observed for **1a** and **2b**.

As discussed in Fig. 3A, the LC assembly of **2a** displays both ferroelectric and paraelectric properties, for which the cyano and amide groups, respectively, are responsible. It is interesting to consider whether these two polar components interfere with each other in their electrical operations. To clarify this point, we used an oriented LC film (thickness, 5 μm) of **2a**, polarly pre-ordered using a (+) DC E-field (10 V μm^{-1}), and an AC E-field (10 Hz, 10 V_{pp} μm^{-1}) was applied periodically (shaded areas in Fig. 3D; each 10 min). SHG signals were sampled when the switching AC E-field was directed parallel or antiparallel to the DC E-field used for the paraelectric polarization. Synchronous with the operation of the AC E-field, the signal intensity quickly changed either positively or negatively depending on the timing for data sampling (Fig. 3D), indicating that a paraelectric motion of the amide component was indeed activated. However, whenever the AC E-field operation was disabled, the SHG activity of the material returned to the original level. Therefore, the paraelectric motion of the amide groups, which allows for the unidirectional columnar orientation (Fig. 2E), does not deteriorate the orientation of the core cyano groups. Namely, in the core–shell columnar assembly of **2a** (Fig. 2, C and D), the hydrogen-bonded amide network with an optimal strength imparts to the polarizable core domain a remnant but electrically invertible axial polarization (Fig. 2A). This is a key design strategy for the long-standing issue of how to realize columnar FLCs.

References and Notes

1. S. T. Largerwall, *Ferroelectric and Antiferroelectric Liquid Crystals* (Wiley-VCH, Weinheim, 1999).
2. R. B. Meyer, L. Liebert, L. Strzelecki, P. Keller, *J. Phys. Lett.* **36**, 69 (1975).
3. H. Takezoe, Y. Takanishi, *Jpn. J. Appl. Phys.* **45**, 597 (2006).
4. R. A. Reddy, C. Tschierske, *J. Mater. Chem.* **16**, 907 (2006).
5. R. A. Reddy *et al.*, *Science* **332**, 72 (2011).
6. N. A. Clark, S. T. Lagerwall, *Appl. Phys. Lett.* **36**, 899 (1980).
7. F. Araoka, H. Hoshi, H. Takezoe, *Phys. Rev. E Stat. Nonlin. Soft Matter Phys.* **69**, 051704 (2004).
8. L. Guo *et al.*, *Phys. Rev. E Stat. Nonlin. Soft Matter Phys.* **84**, 031706 (2011).
9. E. Gorecka *et al.*, *J. Am. Chem. Soc.* **126**, 15946 (2004).
10. K. Kishikawa, S. Nakahara, Y. Nishikawa, S. Kohmoto, M. Yamamoto, *J. Am. Chem. Soc.* **127**, 2565 (2005).
11. Y. Okada *et al.*, *Phys. Rev. E Stat. Nonlin. Soft Matter Phys.* **76**, 041701 (2007).
12. C. F. F. Fitié, W. S. C. Roelofs, M. Kemerink, R. P. Sijbesma, *J. Am. Chem. Soc.* **132**, 6892 (2010).
13. H. Takezoe, K. Kishikawa, E. Gorecka, *J. Mater. Chem.* **16**, 2412 (2006).
14. D. Miyajima *et al.*, *J. Am. Chem. Soc.* **132**, 8530 (2010).
15. H. Bock, W. Helfrich, *Liq. Cryst.* **18**, 707 (1995).
16. A. Jákli, A. Saupe, *Liq. Cryst.* **22**, 309 (1997).
17. D. Kilian *et al.*, *Liq. Cryst.* **27**, 509 (2000).
18. E. Dalcanale, G. Antonioli, M. Riccó, H. Groothues, F. Kremer, *Liq. Cryst.* **27**, 1161 (2000).
19. W. Haase *et al.*, *Liq. Cryst.* **29**, 133 (2002).
20. D. Miyajima *et al.*, *J. Am. Chem. Soc.* **131**, 44 (2009).
21. C. Tschierske, *Chem. Soc. Rev.* **36**, 1930 (2007).
22. B. M. Rosen *et al.*, *Chem. Rev.* **109**, 6275 (2009).
23. D. Miyajima *et al.*, *Angew. Chem. Int. Ed.* **50**, 7865 (2011).
24. Materials and methods are available as supplementary materials on *Science* Online.
25. B. M. Rosen *et al.*, *J. Am. Chem. Soc.* **131**, 17500 (2009).
26. T. Watanabe *et al.*, *Jpn. J. Appl. Phys.* **35**, L505 (1996).
27. E. Gorecka *et al.*, *Phys. Rev. E Stat. Nonlin. Soft Matter Phys.* **73**, 031704 (2006).
28. Y. Okada *et al.*, *Phys. Rev. E Stat. Nonlin. Soft Matter Phys.* **72**, 020701 (2005).
29. S. Horiuchi, Y. Tokura, *Nat. Mater.* **7**, 357 (2008).
30. S. Horiuchi *et al.*, *Nature* **463**, 789 (2010).

Acknowledgments: D.M. thanks the Japan Society for the Promotion of Science for award of a Young Scientist Fellowship. The synchrotron radiation experiments were performed at BL02B2 and BL44B2 in Spring-8 under the Budding Researchers Support Programs and the Priority Nanotechnology Support Program administered by the Japan Synchrotron Radiation Research Institute (Proposal nos. 2008B1777, 2009A1651, and 2009A1699) and with the approval of RIKEN (Proposal no. 20090021).

Supplementary Materials

www.sciencemag.org/cgi/content/full/336/6078/209/DC1
Materials and Methods
Figs. S1 to S8
Reference (*31*)

15 December 2011; accepted 29 February 2012
10.1126/science.1217954